Proceedings of the 2005 IEEE
International Conference on Robotics and Automation
Barcelona, Spain, April 2005

Impact Based Trajectory Planning of a Soccer Ball in a Kicking Robot

Je Youn Choi, Byung Rok So, and Byung-Ju Yi
School of Electrical Engineering and Computer Science
Hanyang University
1271, Sa-1 dong, Sangrok-gu, Ansan, Kyunggi-do, Korea
bj@hanyang.ac.kr

Wheekuk Kim
Department of Control and Instrumentation Engineering
Korea University
208, Seochang-ri, Jochiwon-eup, Chungnam, Korea

Il Hong Suh
Department of information and communication
Hanyang University
17, Haengdang-dong, Seongdong-gu, Seoul, Korea

***Abstract* - This paper deals with the trajectory planning of a soccer ball driven by a kicking robot. The trajectory of a ball is function of its initial velocity, launch angle, and some aerodynamic effect. Specially, the initial velocity is created by an instant impulse given to the ball. The external impulse exerted to a ball by a kicking robot is function of robot geometry and dynamic parameters. Initially, we analyze the external impulses for several kicking postures and simulate trajectories for several different kicking conditions. Based on this observation, a trajectory-planning algorithm of a ball, in which the initial velocity and the launch angle of the ball are calculated for a desired trajectory of the ball, is proposed, and then an external impulse required for that motion is calculated and applied to the kicking simulation. The aerodynamic effect such as drag force and lift force is also incorporated into the dynamic simulation of the soccer ball. A kicking robot has been developed for experimental verification of the proposed analytical methodology. It was shown that experimental result is in good agreement with simulation result within 10% error bound.**

Index Terms - External Impulse, Impact, Soccer, Trajectory planning, Kicking Robot

I. INTRODUCTION

Impact due to collision between the environment and a system occurs at the contact point during the transition from free motion to constrained motion. It can be observed that the human motion consists of continual impact with environment. This phenomenon happens whenever the human body has the topological change of its kinematic structure during the period of impact. It can be visualized in walking, running, grasping or re-grasping an object and sports motion.

Specially, sports players exert larger impact on playing object as compared to routine human-body motions in daily life. At times, excessive impact may cause damage to the joints.

Impulse is defined as the quantitative measure of impact. External impulse is the one that is felt at the contact point. Internal impulse is the one that is felt at the joints. It has been pointed out by experienced players that the posture of human body is an important factor in sports. The amount of external impulse and internal impulse greatly depends on the posture of the human body.

Fig. 1 (a) shows some cases of impact motion in sports.

(a) Impact in sports action (b) Collision to environment

Fig. 1. Impact in sports action

At the moment that the player contacts with the ground or a ball, the amount of external and internal impulses will vary according to the player's posture and mass.

Fig. 1 (b) shows two configurations of a robot manipulator colliding to the environment. In robot control problem, research focus has been on minimizing the impulse experience at the end-effector. Apparently, the configuration (A) is preferred rather than configuration (B) in aspect of minimizing the external impulse experienced at the end-point.

Upon impact, the interacting force at the contact point is difficult to control, and the modeling and control of impact has been considered as an important issue in the field of robotics [1][2]. Several researchers have modeled a robot manipulator and environment as mass-spring-damper systems to understand and simulate the impact phenomena [3-5].

Differently from the above researches, impact dynamics is often regarded discontinuous. Methods to evaluate the impulse have been proposed by several researchers. For a robot system with kinematic redundancy, it is feasible that changing the manipulator configuration can reduce the undesirable effects of the impact. Walker [6] introduced the external impulse model for serial-type robotic manipulator, and proposed a method to reduce the effect of impact by utilizing the self-motion of a kinematically redundant manipulator. Liao and Leu [8] presented the Lagrangian external impact model to derive an impact equation for an industrial manipulator.

When the robotic mechanism collides with environment, the joints of the system also experience impulsive forces or moments. Zheng and Hemami [11] derived the internal impulse model at the joints by using Newton-Euler equations. Wittenburg [10] provides a general methodology

for modeling external and internal impulses. However, his approach is not directly applicable to modeling of the impulse of robot manipulator systems since it is derived in an implicit form. Lee, Yi, Kim and Kwak [12] provided a closed-form internal impulse model for general robot system including, serial-chains, closed chains as well as hybrid-chains.

The objective of this work is an active utilization or control of the external impulse in sports action, specifically kicking motion in soccer. For this, we shortly review the modeling method [9] of external impulse, and perform the external impulse analysis for the kicking motion in soccer. Furthermore, a trajectory-planning algorithm of a ball, in which the initial velocity and the launch angle of the ball are calculated for a desired trajectory of the ball, will be introduced. The aerodynamic effect such as drag force and lift force is also considered. We carry out numerical simulation to verify the effectiveness of the proposed analytical methodology.

II. External Impulse Modeling

As a basic model, we choose the leg model of a soccer player. It can be modeled as a planar system having three links as shown in Fig. 2. The links represent the thigh, the shank, and the foot, respectively. The point P represents the impact point between a ball and the foot of a soccer player.

$\boldsymbol{F}_{ext}$ is the impulsive external force at the contact point. Most generally, the impact is partially elastic in the range of $0 < e < 1$. When the coefficient of restitution e is known, the relative velocity of colliding bodies can be obtained immediately after the impact. The component of the increment of relative velocity along a vector $\mathbf{n}$ that is normal to the contact surface is given by [10]

$$\left(\Delta\boldsymbol{\upsilon}_1 - \Delta\boldsymbol{\upsilon}_2\right)^T \boldsymbol{n} = -(1+e)\left(\boldsymbol{\upsilon}_1 - \boldsymbol{\upsilon}_2\right)^T \boldsymbol{n}\,, \tag{1}$$

where $\boldsymbol{\upsilon}_1$ and $\boldsymbol{\upsilon}_2$ are the absolute velocities of the colliding bodies immediately before impact, and $\Delta\boldsymbol{\upsilon}_1$ and $\Delta\boldsymbol{\upsilon}_2$ are the velocity increments immediately after impact.

The external impact modeling methodology for the serial-type system is introduced by Walker [6-7]. When a robot system interacts with environment, the dynamic model of general robot systems is given as

$$\boldsymbol{T} = [\boldsymbol{I}^*_{\phi\phi}]\ddot{\boldsymbol{\phi}} + \dot{\boldsymbol{\phi}}^T[\boldsymbol{P}^*_{\phi\phi\phi}]\dot{\boldsymbol{\phi}} - [\boldsymbol{G}^{\upsilon_I}_{\phi}]^T \boldsymbol{F}_{ext}\,, \tag{2}$$

where $\boldsymbol{F}_{ext}$ is the impulsive external force at the contact point. $[\boldsymbol{G}^{\upsilon_I}_{\phi}]$ denotes the Jacobian (i.e. the 1st-order Kinematic Influence Coefficient; KIC), relating the contact point's velocity $\boldsymbol{\upsilon}_I$ to the independent joint velocities.

Integration of the dynamic model given in Eq. (2) over contacting time interval gives

$$\begin{aligned}\int_{t_0}^{t_0+\Delta t} \boldsymbol{T}dt = &\int_{t_0}^{t_0+\Delta t} [\boldsymbol{I}^*_{\phi\phi}]\ddot{\boldsymbol{\phi}}\; dt + \int_{t_0}^{t_0+\Delta t} \dot{\boldsymbol{\phi}}^T[\boldsymbol{P}^*_{\phi\phi\phi}]\dot{\boldsymbol{\phi}}\; dt \\ &- \int_{t_0}^{t_0+\Delta t} [\boldsymbol{G}^{\upsilon_I}_{\phi}]^T \boldsymbol{F}_{ext} dt.\end{aligned} \tag{3}$$

Since the positions and velocities are assumed finite all the time during impact, the integral term involving $\dot{\boldsymbol{\phi}}^T[\boldsymbol{P}^*_{\phi\phi\phi}]\dot{\boldsymbol{\phi}}$ becomes zero as Δt goes to zero, as does the term involving actuation input $\boldsymbol{T}$. Thus, we obtain the following simple expression

$$[\boldsymbol{I}^*_{\phi\phi}]\left(\dot{\boldsymbol{\phi}}(t_0+\Delta t) - \dot{\boldsymbol{\phi}}(t_0)\right) = [\boldsymbol{G}^{\upsilon_I}_{\phi}]^T \tilde{\boldsymbol{F}}_{ext} \tag{4}$$

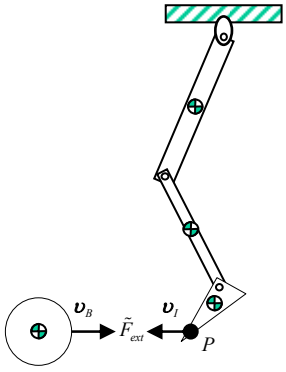

Fig. 2 Kicking model of a human leg

where $\tilde{\boldsymbol{F}}_{ext} = \int_{t_0}^{t_0+\Delta t} \boldsymbol{F}_{ext}\, dt$ is defined as the external impulse at the contact point. Thus, the velocity increment of the joint variables is

$$\Delta\dot{\boldsymbol{\phi}} = [\boldsymbol{I}^*_{\phi\phi}]^{-1}[\boldsymbol{G}^{\upsilon_I}_{\phi}]^T \tilde{\boldsymbol{F}}_{ext} \tag{5}$$

and the velocity increment at the contact point is obtained by the following kinematic relationship.

$$\Delta\boldsymbol{\upsilon}_I = [\boldsymbol{G}^{\upsilon_I}_{\phi}]\Delta\dot{\boldsymbol{\phi}} = [\boldsymbol{G}^{\upsilon_I}_{\phi}][\boldsymbol{I}^*_{\phi\phi}]^{-1}[\boldsymbol{G}^{\upsilon_I}_{\phi}]^T \tilde{\boldsymbol{F}}_{ext}\,, \tag{6}$$

$$\Delta\boldsymbol{\upsilon}_B = [\boldsymbol{G}^{B}_{\phi}]\Delta\dot{\boldsymbol{\phi}} = [\boldsymbol{G}^{B}_{\phi}][\boldsymbol{I}^*_{\phi\phi B}]^{-1}[\boldsymbol{G}^{B}_{\phi}]^T(-\tilde{\boldsymbol{F}}_{ext})\,, \tag{7}$$

where $[\boldsymbol{G}^{B}_{\phi}]$ and $[\boldsymbol{I}^*_{\phi\phi B}]$ denotes the Jacobian, the inertia matrix of the ball, respectively.

Substitution of Eq. (6) and Eq. (7) into Eq. (1) gives

$$\begin{aligned}&\left\{\left([\boldsymbol{G}^{\upsilon_I}_{\phi}][\boldsymbol{I}^*_{\phi\phi I}]^{-1}[\boldsymbol{G}^{\upsilon_I}_{\phi}]^T + [\boldsymbol{G}^{B}_{\phi}][\boldsymbol{I}^*_{\phi\phi B}]^{-1}[\boldsymbol{G}^{B}_{\phi}]^T\right)\tilde{\boldsymbol{F}}_{ext}\right\}^T \boldsymbol{n} \\ &\qquad = -(1+e)\left(\boldsymbol{\upsilon}_I - \boldsymbol{\upsilon}_B\right)^T \boldsymbol{n}\end{aligned} \tag{8}$$

Assuming that no friction exists on the contacting surface, impulse always acts at the contact point along the normal vector $\boldsymbol{n}$. Thus, we have

$$\tilde{\boldsymbol{F}}_{ext} = \tilde{F}_{ext}\boldsymbol{n}\,. \tag{9}$$

Substituting Eq. (9) into Eq. (8), we derive the magnitude of the impulse as follows:

$$\tilde{F}_{ext} = \frac{-(1+e)(\boldsymbol{\upsilon}_I - \boldsymbol{\upsilon}_B)^T \boldsymbol{n}}{\boldsymbol{n}^T\{[\boldsymbol{G}^{\upsilon_I}_{\phi}][\boldsymbol{I}^{\bullet}_{\phi\phi I}]^{-1}[\boldsymbol{G}^{\upsilon_I}_{\phi}]^T + [\boldsymbol{G}^{B}_{\phi}][\boldsymbol{I}^{\bullet}_{\phi\phi B}]^{-1}[\boldsymbol{G}^{B}_{\phi}]^T\}\boldsymbol{n}}\,, \tag{10}$$

where $[\boldsymbol{I}^*_{\phi\phi I}]$ and $[\boldsymbol{I}^*_{\phi\phi B}]$ denotes the moment inertia of the foot and the soccer ball, respectively. Specifically, when the ball is regarded as a particle, the moment inertia of the ball is given as

$$[\boldsymbol{I}^*_{\phi\phi B}] = \begin{bmatrix} m_B & 0 & 0 \\ 0 & m_B & 0 \\ 0 & 0 & m_B \end{bmatrix}, \tag{11}$$

where m_B denotes the mass of the ball.

III. Models of Aerodynamic Forces

According to the external impulse applied to the soccer ball, it will have initial linear velocity and angular velocity. After the onset of the motion, various aerodynamic forces as well as the gravity load will affect the flying ball.

First, the drag force denoted by

$$F_D = C_D A\frac{\rho U_\infty^2}{2}\,, \tag{12}$$

is applied to ball due to the airflow against the ball. It is directed to the negative direction of the ball's velocity. There are two kinds of drag forces; surface drag force and pressure drag force in the shape of sphere. Eq. (12) includes both

effects. In Eq. (12), C_D, A, ρ and U_∞ denote the drag force coefficient, the cross sectional area of the ball, the air density at standard state ($15^\circ C$, 1013hpa) and the velocity of the airflow, respectively.

The flying object also receives a force in the perpendicular direction of the ball's velocity when it rotates. This phenomenon is call "Magnus effect". This effect causes the ball to take turn-right or turn-left or lift-up or lift-down. We call this force as a lift force denoted by

$$F_L = C_L A \frac{\rho V^2}{2}. \quad (13)$$

Note that the coefficients C_D and C_L are measured based on Reynolds number represented by

$$N_{Red} = \frac{\rho V D}{\mu},$$

where D is the diameter of sphere and μ is coefficient of air viscosity. Fig. 3 depicts these aerodynamic forces applied to the flying ball with a linear velocity and a rotating angular velocity.

In case of $N_{Red} < 1$, the Drag force is given analytically as

$$F_D = 3\pi\mu V D, \quad (14)$$

where $C_D = \frac{24}{N_{Red}}$.

Generally, when the ball receives an impact, three rotational motions are developed simultaneously as shown in Fig. 4.

This complex rotation creates a variety of trajectories of the ball. The direction of the lift force is perpendicular to the directions of both the ball's linear velocity and the rotating velocity. Fig. 5 denotes the two examples of the resulting Lift force.

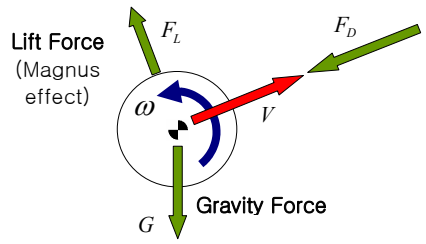

Fig. 3 Aerodynamic forces applied to a flying ball

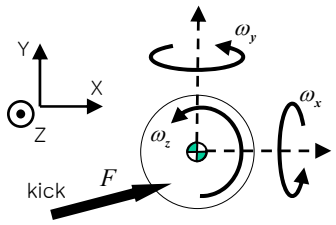

Fig. 4 3-DOF rotational motions

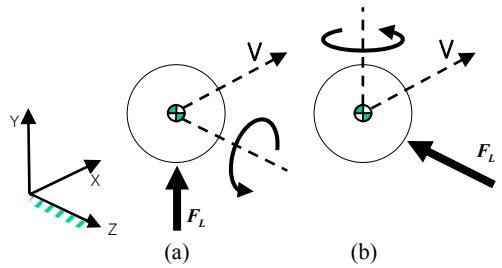

Fig. 5 Direction of the lift force according to the rotational direction

IV. External Impulse Model Considering Friction

When an impulsive external force is exerted on the surface of a ball, the force can be resolved into two components, normal to the surface and tangential to the surface. If the friction is negligible on the surface of the ball, the direction of the external impulse will be toward the center of the ball. Eq.(10) denotes this case. However, when the friction is considerable, there is additional external impulse along the surface tangential direction.

As shown in Fig.6, let $\boldsymbol{F}_n$ and $\boldsymbol{F}_t$ be the surface normal and surface tangential forces applied to the ball. $\boldsymbol{F}_n$ is the amount that is always transmitted to the normal direction, but the maximum friction force $\boldsymbol{F}_f$ along the tangential direction is associated with $\mu_f \boldsymbol{F}_n$. Thus, when $\boldsymbol{F}_t$ exceeds the magnitude of $\mu_f \boldsymbol{F}_n$, a slipping phenomenon starts.

Finally, the total external impulse exerted on the ball during the impact period will be a vector sum of $\tilde{\boldsymbol{F}}_n (= \int_{t_0}^{t_0+\Delta t} \boldsymbol{F}_n \mathrm{d}t)$ and $\tilde{\boldsymbol{F}}_f (= \int_{t_0}^{t_0+\Delta t} \boldsymbol{F}_f \mathrm{d}t)$.

Now, it is necessary to identify the directions of $\tilde{\boldsymbol{F}}_n$ and $\tilde{\boldsymbol{F}}_f$ (or, $\boldsymbol{F}_n$ and $\boldsymbol{F}_f$). First of all, the direction of $\boldsymbol{F}_n$ can be easily computed since the angle α between $\boldsymbol{F}$ and $\boldsymbol{F}_n$ (Fig. 6) can be computed when the position of the contact point is given with respect to the body-fixed ball coordinate. Secondly, noting that the three vectors $\boldsymbol{F}$, $\boldsymbol{F}_n$ and $\boldsymbol{F}_f$ are in the same plane, we have

$$\boldsymbol{F} \cdot (\boldsymbol{F}_n \times \boldsymbol{F}_f) = 0 \quad (15)$$

and

$$\boldsymbol{F}_n \cdot \boldsymbol{F}_f = 0. \quad (16)$$

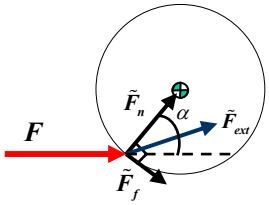

Fig. 6 External impulse model considering friction

Let the unit vectors of $\boldsymbol{F}$, $\boldsymbol{F}_n$, and $\boldsymbol{F}_t$ be expressed as

$$\boldsymbol{F}_u = \begin{bmatrix} f_{ux} & f_{uy} & f_{uz} \end{bmatrix}^T,$$

$$\boldsymbol{N} = \begin{bmatrix} n_x & n_y & n_z \end{bmatrix}^T,$$

and

$$\boldsymbol{T} = \begin{bmatrix} t_x & t_y & t_z \end{bmatrix}^T,$$

where $\boldsymbol{F}_u$ and $\boldsymbol{N}$ are known, and the components of $\boldsymbol{T}$ need to be found. The property of a unit vector gives

$$t_x^2 + t_y^2 + t_z^2 = 1. \quad (17)$$

Now, the components of $\boldsymbol{T}$ can be obtained from Eq. (15), Eq. (16), and Eq. (17)

When $\boldsymbol{F}_t$ is smaller than $\mu_f \boldsymbol{F}_n$, there is no slip. Accordingly, we have

$$\boldsymbol{F}_f = \boldsymbol{F}_t, \quad (18)$$

where

$$\boldsymbol{F}_t = \boldsymbol{F} - \boldsymbol{F}_n. \quad (19)$$

However, slip occurs when F_t is larger than $\mu_f F_n$. In this case, the amount of transmitted impulse to the ball is

$$\tilde{F}_f = \left|\mu_f \tilde{F}_n\right| \boldsymbol{T}, \tag{20}$$

where

$$\left|\tilde{F}_n\right| = \left|\tilde{F}\right| \cos\alpha,$$

Consequently, the frictional external impulse $\tilde{F}_f$ creates an external torque impulse about the center of the ball. It is given by

$$\tilde{\tau} = \boldsymbol{r} \times \tilde{F}_f = [I^*_{\phi\phi B}] \Delta\omega_0, \tag{21}$$

which provides the initial angular velocity ω_0 of the ball. In Eq. (21), $\boldsymbol{r}$ denotes a vector directing from the center of the ball to the attack point.

V. Simulation

A. Analysis of external impulse

Sport players have to control the amount of impact when playing with a ball. At the instant of impact, the external impulse exerted on the ball decides the initial motion of the ball. However, Eq. (10) illustrates a fact that external impulse is associated with the configuration of the leg, the impact velocity, and also the dynamic parameters of the leg. Therefore, a thorough analysis is necessary to design the content of the external impulse.

As an example, we attempt to analyze the impulse characteristics at the kicking action. Table 1 denotes the kinematic and dynamic parameters of the leg model of the human body in the planar domain.

Fig. 7 shows the three postures of the kicking motion with the magnitudes of the impulses depicted at the end of the foot. For the case (a), the angle of the ankle is 0 degrees relative to the horizontal ground, the case (b) has 20 degrees and the case (c) has 45degrees.

Also the attack angle of the foot against the ball is given 30 degrees relative to the horizontal ground. Thus, the direction of external impulse is also identical to this direction if the direction of the external impulse is toward the center of the ball. It can be observed that the amount of the external impulse becomes smaller for the small angle of the ankle.

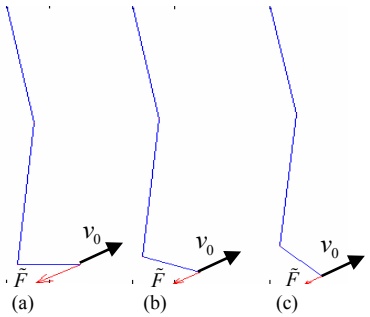

Fig. 7 External impulse of kicking motion

Table 1. The size and inertia of the human model

	Length(m)	Mass(kg)	Inertia($kg \cdot m^2$)
Thigh	0.371	7	0.08
Shank	0.443	3	0.049
Foot	0.145	1	0.0018

Table 2. External impulse

	case (a)	case (b)	case (c)
X (N·s)	1.346	0.817	0.559
Y (N·s)	0.777	0.472	0.323
Total (N·s)	1.554	0.944	0.646

This result tells that the posture of straight ankle transmits large external impulse to the ball. External impulses of the three cases are listed in Table 2 when the velocity of the foot is given 1 [m/s].

B. Simulation of a soccer ball's trajectory

Based on the Newton's equation and Euler's equation, the dynamics of ball can be expressed as

$$\boldsymbol{F} = m_b \boldsymbol{a}_b = \boldsymbol{F}_D + \boldsymbol{F}_L + m_b \boldsymbol{g}, \tag{22}$$

$$\boldsymbol{\tau} = [{}^c\boldsymbol{I}]{}^c\dot{\boldsymbol{\omega}} + {}^c\boldsymbol{\omega} \times [{}^c\boldsymbol{I}]{}^c\boldsymbol{\omega}, \tag{23}$$

where ${}^c\boldsymbol{\omega}$ is the angular velocity vector referenced to the ball coordinate. Assuming that the ball is a hollow spherical shell, the inertia tensor $[{}^c\boldsymbol{I}]$ of the soccer ball referenced to the ball coordinate is given as

$$[{}^c\boldsymbol{I}] = \begin{bmatrix} 2m_b r^2/3 & 0 & 0 \\ 0 & 2m_b r^2/3 & 0 \\ 0 & 0 & 2m_b r^2/3 \end{bmatrix},$$

where r denotes radius of ball.

If the ball is modeled as a particle, it is not influenced by the Drag and Lift forces. Thus, $\boldsymbol{F}_D$ and $\boldsymbol{F}_L$ are zero. However, if the ball is a rigid body, $\boldsymbol{F}_D$ and $\boldsymbol{F}_L$ will be continuously changing during its motion period.

The position and orientation of the soccer ball with respect to the global reference coordinate will be obtained by numerical integration of the Newton-Euler equations. During the motion, the coefficients of Drag force and Lift force will be continuously updated.

After the onset of the impact, the soccer ball starts flying or rolling. The aerodynamic forces and the gravity load dominate the trend of the ball's trajectory. Also, depending upon the location of the impact given to the ball, the characteristics of initial velocity of the ball are decided. In what follows, the coefficient of the friction on the surface of the soccer ball is assumed as 0.4.

Fig. 8 denotes four trajectories of the ball in the two-dimensional space. It is shown that the Drag force hinders the ball's movement, and thus the traveled distance is shorter than that of no Drag force. Also when the impact creates some spin of the ball such as a top spin and a back spin, the ball is influenced by the Lift force. The back spin yields the largest height. On the other hand, the top spin yields the lowest height but substantially shorter arrival distance. The results are coincident to the human intuition.

Fig. 9 represents the simulation results for the back spin due to the impact at three different positions. Assume that the three cases have the same velocities and configurations of the foot. The case 3 having the largest back spin travels farthest and highest. Table 3 shows the contents of the linear and angular motions after the onset of the impact.

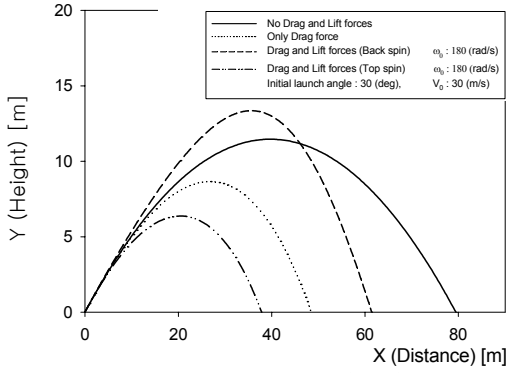

Fig. 8 Planar trajectory of a flying ball

In general 3-dimensional case, the ball has three rotational motions. Fig. 10 shows the trajectories of the soccer ball when the impact is given to the ball at three different positions. The middle trajectory is created when the impact is given to the center-lower part of the ball. The ball has a forward linear velocity with a back spin about the axis A, as shown in Fig. 11 (a). Thus, the ball's trajectory is two-dimensional. The left trajectory corresponds to the case that the impact is given to the right-lower part of the ball. The ball has a forward linear velocity with a back spin about the axis B, as shown in Fig. 11 (b). Thus, the ball's trajectory turns to the left. Finally, the curved trajectory on the right side is generated by the initial angular velocity history given in Fig. 11 (c). The simulation data and assumptions are given in Table 3.

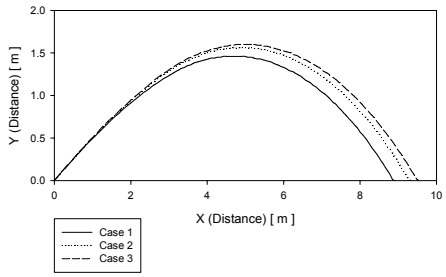

(a)

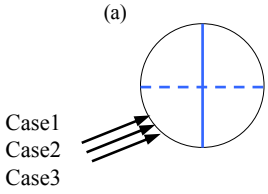

(b)

	Linear velocity	Angular velocity	launch angle(deg)	Foot vel[m/s]
Case 1	12.82	37.9	28.62	1.2
Case 2	12.81	54.2	28.67	1.2
Case 3	12.8	69.8	28.7	1.2

(c)

Fig. 9 Trajectory for different impact position

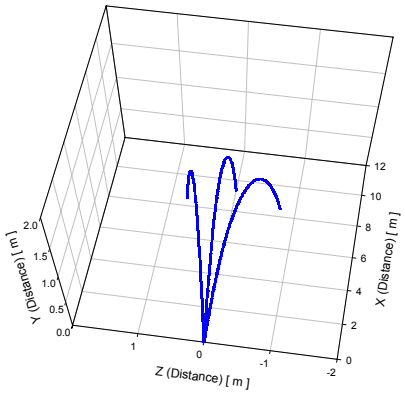

Fig. 10 Three-dimension trajectory of a flying ball

Table 3. Simulation data

External disturbance wind	None
Air density	1.220 [Kg/m^3]
Radius of ball	0.1 [m]
Mass of ball	0.45[Kg]
Coefficient of Viscosity	1.8E-5
Gravity acceleration	9.81 [m/s^2]
Foot velocity	1.2 [m/s]

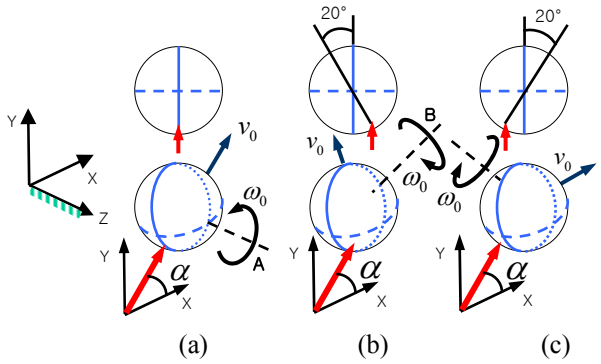

Fig. 11 Initial velocity profiles of the soccer ball (back and side view)

C. *Preliminary trajectory planning of the soccer ball*

The foremost and fundamental skill in the soccer will be the timely kick such that a soccer ball will arrive at the boundary of another player in good time. This can be easily understood from a simple particle motion under gravity. When a particle is launched with an initial velocity v_o as shown in Fig. 12, the arrival distance x and the height y at any arbitrary time or x position can be expressed as follows

$$X = (v_o \cos\theta)t \tag{24}$$

$$Y = (v_o \sin\theta)t - 0.5gt^2 \tag{25}$$

and Eq. (24) can be rewritten as

$$X/t = v_o \cos\theta$$

which implies that the arrival distance x and the arrival time t are functions of both the initial velocity of the ball and the launch angle.

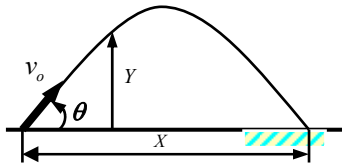

Fig. 12 Trajectory of a particle under the gravity field

However, in practice, the trajectory of the soccer ball won't have such a closed-form solution as the particle because the Newton-Euler equations are highly nonlinear due to the aerodynamics forces. Thus, the trajectory planning of the soccer ball should be based on some sort of learning algorithms. Here, one simple offline training algorithm will be explained.

We desire to control the arrival time (t) and the arrival distance (x) of the soccer ball. For this, we initially employ a simple control algorithm shown in Fig. 13 to control the arrival time and the arrival distance of the ball. A reinforcement learning algorithm [16] is embedded in the controller to satisfy the given goal of the soccer ball's trajectory. The flow chart of the reinforced learning control is shown in Fig. 14.

In the simulation, the closed-form solution of the particle motion, given in Eq. (24) and (25), is employed as the nominal

values, and the trajectory under the Drag force is also used as the minimum bound of the soccer ball's trajectory. For simplicity, we assume only a linear motion without any spin. The learning scheme is applied to both the arrival distance and the arrival time. The simulation data are the same as those of Fig. 8.

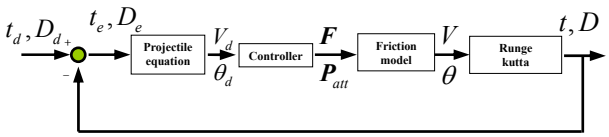

Fig. 13 Block diagram for controlling
the arrival time and arrival distance of a ball

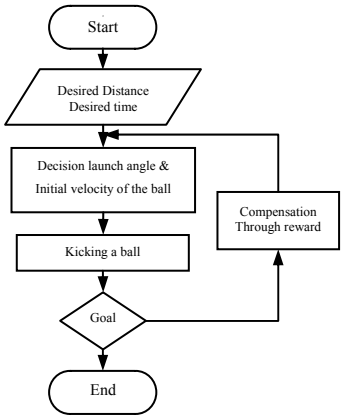

Fig. 14 Flowchart for the reinforced learning control

The desired x and t are given three different sets. First, Fig.15 (a) and (b) denote distance and time error when the desired goals are given 30 meters and 1.5 seconds. Second, Fig.15 (c) and (d) are for 50 meters and 2 seconds. Third, Fig.15 (e) and (f) denote the case of 100 meters and 3 seconds. Fig. 15 shows that the each error sets between the nominal values and the actual values are decreasing by employing the reinforced learning scheme. We can see that the number of iterations is increased as the goal distance and time get high values.

Using the same learning algorithm, planning of the height at any position x and a planned spin kick can be also taken into account for more sophisticated trajectories of the soccer ball.

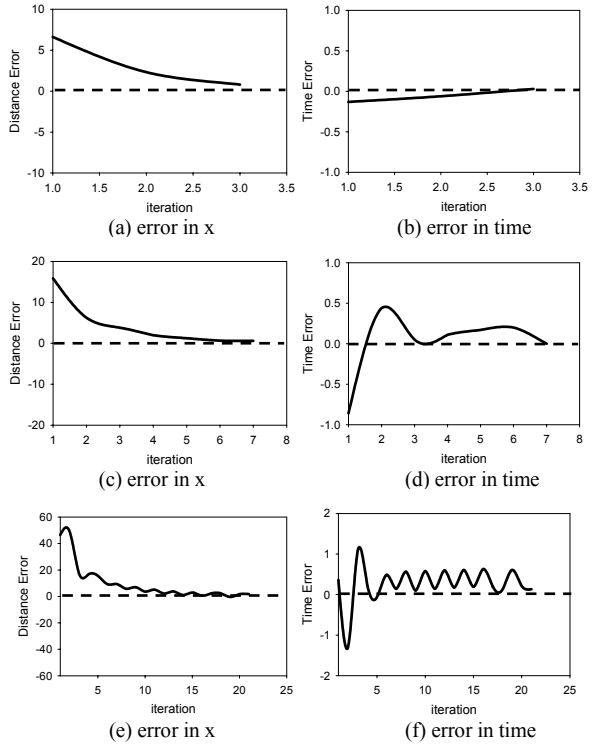

(a) error in x (b) error in time

(c) error in x (d) error in time

(e) error in x (f) error in time

Fig. 15. Trajectory planning of the soccer ball

D. Experimental result

Fig. 16 shows the experimental setup for kicking experimentation. An AC motor is used at hip joint and a DC motor is used at the knee joint, respectively. Kicking motion usually requires large torque at motor. So, we employ a motor with large torque capacity and high power. Table 6 denotes the kinematic and dynamic parameters of the experimental test bed. Table 4 represents the experimental result for the impact at three different positions. Three cases have the same foot velocities and foot configurations at the moment of impact.

When the leg robot kicks the 50 degree position, the soccer ball travels farthest and highest. The second experimentation is performed for different impact velocities, but with the same impact angle. Table 8 and Table 5 show that the error between the experimentation and the simulation is within 10%. The discrepancy between the simulation and experiment is due to in part assumption of imprecise modeling of the soccer ball's deflection and energy consumption upon impact, and imprecise modeling of aerodynamic effect. However, the result is acceptable since the ratio of the error is not that critical in estimation of the soccer ball's trajectory.

(a) Side view (b) Isometric view

Fig. 16 Experimental Setup for Kicking a Soccer Ball

Table 4. Experimental result for different impact angles

Impact point of ball θ [deg]	**Foot velocity [m/s]**	**Distance [m]**	
		Experiment	***Simulation***
30	2.2	3.9	3.75
40	2.2	6.5	6.86
50	2.2	7.5	8

Table 5. Experimental result for different impact velocities

Attack angle [deg]	**Impact point of ball θ [deg]**	**Foot velocity [m/s]**	**Distance [m]**	
			Experiment	***Simulation***
20	50	2.2	7.5	8
20	50	2.0	6.3	6.75
20	50	1.8	5.3	5.53

Table 6. Kinematic, dynamic parameters

	Thigh	**Shank**	**Foot**
Link length (m)	0.4	0.396	0.22
Weight (kg)	1.712	1.074	0.57
Inertia (kg·m²)	0.02305	0.01413	0.00055
Mass center (m)	0.2	0.198	0.073

VI. CONCLUSIONS

Now, many human-like robots have been reported worldwide. Thus, as the concept of Humanoid becomes popular, we might dream so often the useful applications of Humanoid. As one of those, robot sports can be one potential application. However, current technology is far from controlling impact occurring in various sport actions. In this paper, we have dealt with impulse modeling of the kicking motion and the trajectory planning of the soccer ball with consideration of the arrival time and the arrival distance of the ball. Even though the leg model of this work was confined to 2-dimensional case, the simulated trajectory of the soccer ball was coincident to the human's experiences.

As the future work, more updated human body model will be taken in account to allow more general trajectory planning of the soccer ball. Also, we will develop a biped mechanism and a full-body Humanoid for experimental verification of the proposed algorithm and develop more advance reinforcement learning algorithm to control various trajectories. The analytic tools and practices developed in this work are expected to be useful in the impulse analysis of several kinds of sports action as well as robot applications with emphasis on impact control.

REFERENCES

[1] R. M. Brach, "Classical planar impact theory and the tip impact of a slender rod," International Journal of Impact Engineering, Vol. 13, No. 1, pp. 21-33, 1993.

[2] G. Ferretti, G. Magnani, and A. Zavala Rio, "Impact modeling and control for industrial manipulators," *IEEE Control System Magazine*, Vol. 18, No. 4, pp. 65-71, 1998.

[3] J. K. Mills and C. V. Nguyen, "Robotic manipulator collisions: Modeling and simulation," *ASME Journal of Dynamic Systems, Measurement, and Control*, Vol. 114, No. 4, pp. 650-659, 1992.

[4] A. S. Yigit, "The effect of flexibility on the impact response of a two-link rigid-flexible manipulator," *Journal of Sound and Vibration*, Vol. 177, No. 3, pp. 349-361, 1994.

[5] K. Youcef-Toumi and D.A. Gutz, "Impact and force control," *Proceedings of the IEEE Conference on Robotics and Automation*, pp. 410-416, 1989.

[6] I. D. Walker, "The use of kinematic redundancy in reducing impact and contact effects in manipulation," *Proceeding of 1990 IEEE Conference on Robotics and Automation*, pp. 434-439, 1990.

[7] I. D. Walker, "Impact configurations and measures for kinematically redundant and multiple armed robot systems," *IEEE Trans. on Robotics Automation*, Vol.12, No.5, pp. 670-683, 1994.

[8] H. T. Liao and M. C. Leu, "Analysis of impact in robotic peg-in-hole assembly," *Robotica*, Vol. 16, No. 3, pp. 347-356, 1998.

[9] Y. Nakamura and M. Ghodoussi, "Dynamic computation of closed-link robot mechanisms with non-redundant and redundant actuators," *IEEE Transaction on Robotics and Automation*, Vol. 5, No. 3, pp. 294-302, 1989.

[10] J. Wittenburg, Dynamics of systems of rigid bodies, Stuttgart, B.G. Teubner, 1977.

[11] Y. F. Zheng and H. Henami, "Mathematical modeling of a robot collision with its environment," *Journal of Robotic System*s, Vol. 2, No. 3, pp. 289-307, 1985.

[12] S. H. Lee, B. J. Yi, S. H. Kim, and Y. K. Kwak, "Modeling and analysis of internal impact for general classes of robotic mechanism," *Proceedings of the 2000 IEEE/RSJ International Conference on Robotics and Systems*, pp. 1955-1962, 2000.

[13] R. A. Freeman and D. Tesar, "Dynamic modeling of serial and parallel mechanisms/robotic systems, Part I-Methodology, Part II-Applications," *Proceedings on 20th ASME Biennial Mechanisms Conference, Trends and Development in Mechanisms, Machines, and Robotics*, Orlando, FL, DE-Vol. 15-3, pp. 7-27, 1988.

[14] B. J. Son, J. S. Maeng and S. H. Lee, *Fluid dynamics*, Seoul, Hee Jung Dang, 1992.

[15] B. R. So, B.-J. Yi and W. K. Kim, "Impulse analysis its applications to dynamic environment," ASME Biennial Mechanism, Montreal, Canada, 2002.

[16] Richard S. Sutton and Andrew G. Barto, "Reinforcement Learning," The MIT Press, Third edition, 2000.

[17] Ming. A, Teshima. T, Takayama. T and Kajitani. M, "Control of a New Golf Swing Robot with Considering Hitting a Ball", *Systems, Man, and Cybernetics, 2001 IEEE International Conference on* , Vol. 1, pp. 365 - 370, 2001.